

Interference between two indistinguishable electrons from independent sources

I. Neder¹, N. Ofek¹, Y. Chung², M. Heiblum¹, D. Mahalu¹ & V. Umansky¹

Very much like the ubiquitous quantum interference of a single particle with itself¹, quantum interference of two independent, but indistinguishable, particles is also possible. For a single particle, the interference is between the amplitudes of the particle's wavefunctions, whereas the interference between two particles is a direct result of quantum exchange statistics. Such interference is observed only in the joint probability of finding the particles in two separated detectors, after they were injected from two spatially separated and independent sources. Experimental realizations of two-particle interferometers have been proposed^{2,3}; in these proposals it was shown that such correlations are a direct signature of quantum entanglement⁴ between the spatial degrees of freedom of the two particles ('orbital entanglement'), even though they do not interact with each other. In optics, experiments using indistinguishable pairs of photons encountered difficulties in generating pairs of independent photons and synchronizing their arrival times; thus they have concentrated on detecting bunching of photons (bosons) by coincidence measurements^{5,6}. Similar experiments with electrons are rather scarce. Cross-correlation measurements between partitioned currents, emanating from one source^{7–10}, yielded similar information to that obtained from auto-correlation (shot noise) measurements^{11,12}. The proposal of ref. 3 is an electronic analogue to the historical Hanbury Brown and Twiss experiment with classical light^{13,14}. It is based on the electronic Mach–Zehnder interferometer¹⁵ that uses edge channels in the quantum Hall effect regime¹⁶. Here we implement such an interferometer. We partitioned two independent and mutually incoherent electron beams into two trajectories, so that the combined four trajectories enclosed an Aharonov–Bohm flux. Although individual currents and their fluctuations (shot noise measured by auto-correlation) were found to be independent of the Aharonov–Bohm flux, the cross-correlation between current fluctuations at two opposite points across the device exhibited strong Aharonov–Bohm oscillations, suggesting orbital entanglement between the two electron beams.

In many ways, experiments with electrons are easier than those with photons. Injecting electrons from an extremely cold and degenerate fermionic reservoir produces a highly ordered beam of electrons that is totally noiseless¹⁷; hence, a high coincidence rate is achieved without the need to synchronize the arrival times of the electrons. As each electron has a definite energy (Fermi energy) and momentum (Fermi momentum), electrons can be made indistinguishable by injecting them from two equal voltage sources. Moreover, because the coherence length of the electrons ('wave packet width' or 'spatial size') is determined by the source voltage (at low temperature), a very small source voltage ensures the presence of a single electron at a time in the interferometer, preventing electron–electron interactions. However, the small voltage leads to an exceedingly small electrical

current and to minute fluctuations, making the measurements extremely difficult to perform.

A diagram of our experiment is shown in Fig. 1a (ref. 2). Two independent, separated, sources of electrons (S1 and S2) inject ordered, hence noiseless, electrons towards each other. Each stream passes through a beam splitter (A and B), and splits into two negatively correlated partitioned streams (if an electron turns right, a hole is injected to the left). Both sets of the two partitioned streams join each other at two additional beam splitters (C and D), interfere there and generate altogether four streams that are collected by drains D1–D4. Hence, every electron emitted by either S1 or S2 eventually arrived at one of the four drains. Consider now the event where one electron arrives at D2 and the other arrives at D4. There are two quantum mechanical probability amplitudes contributing to this event: S1 to D2 and S2 to D4; or, alternatively, S1 to D4 and S2 to D2. These two 'two-particle' events can interfere because they are indistinguishable. Because in the two possible events the electrons travel along different paths (thus accumulating different phases), the joint probability of one arriving at D2 and the other at D4 contains the total phase of all paths—as we show below.

The two wavefunctions, corresponding to the incoming states from each of the two sources Ψ_{S_i} , can be expressed in the basis of the outgoing states at the four drains ψ_{D_j} . Assuming, as in the experiment, that every beam splitter is half reflecting and half transmitting, its unitary scattering matrix M (that ties the input and output states) can be taken as: $M = \begin{bmatrix} r & t \\ t' & r' \end{bmatrix} = \frac{1}{\sqrt{2}} \begin{bmatrix} i & 1 \\ 1 & i \end{bmatrix}$. Considering the phases of the four possible paths ϕ_1, \dots, ϕ_4 :

$$\Psi_{S1}(x) = \frac{1}{2} [ie^{i\phi_1}\psi_{D1}(x) - e^{i\phi_1}\psi_{D2}(x) + ie^{i\phi_2}\psi_{D3}(x) + e^{i\phi_2}\psi_{D4}(x)] \quad (1a)$$

$$\Psi_{S2}(x) = \frac{1}{2} [ie^{i\phi_3}\psi_{D1}(x) + e^{i\phi_3}\psi_{D2}(x) + ie^{i\phi_4}\psi_{D3}(x) - e^{i\phi_4}\psi_{D4}(x)] \quad (1b)$$

As, in this set-up, each electron is not allowed to interfere with itself, only particle statistics could cause interference. Because of the fermionic property of electrons, the total two-particle wavefunction must be the antisymmetric product of equation (1a) and equation (1b):

$$\Psi_{\text{total}}(x_1, x_2) = \frac{1}{\sqrt{2}} [\Psi_{S1}(x_1) \Psi_{S2}(x_2) - \Psi_{S2}(x_1) \Psi_{S1}(x_2)] \quad (2)$$

with x_1 and x_2 any two locations in the interferometer. Substituting equation (1) in equation (2) leads to 24 terms, expressing the probability amplitude for one electron at x_1 and another at x_2 . As we wish to concentrate on correlations between drains, we write Ψ_{total} using the notation $\psi_{D_i D_j} \equiv \frac{1}{\sqrt{2}} [\psi_{D_i}(x_1) \psi_{D_j}(x_2) - \psi_{D_j}(x_1) \psi_{D_i}(x_2)]$ for an antisymmetric state, in which one electron heads to D_i and another

¹Braun Center for Submicron Research, Department of Condensed Matter Physics, Weizmann Institute of Science, Rehovot 76100, Israel. ²Department of Physics, Pusan National University, Busan 609-735, Korea.

to D_j . The two-particle wavefunction is:

$$\Psi_{\text{total}}(x_1, x_2) = \frac{i}{2} (e^{i(\phi_1 + \phi_3)} \psi_{D1D2} - e^{i(\phi_2 + \phi_4)} \psi_{D3D4}) + \frac{i}{2} e^{i(\phi_1 + \phi_2 + \phi_3 + \phi_4)} \left[\sin\left(\frac{\Phi_{\text{total}}}{2}\right) (\psi_{D2D4} - \psi_{D1D3}) - \cos\left(\frac{\Phi_{\text{total}}}{2}\right) (\psi_{D2D3} + \psi_{D1D4}) \right] \quad (3)$$

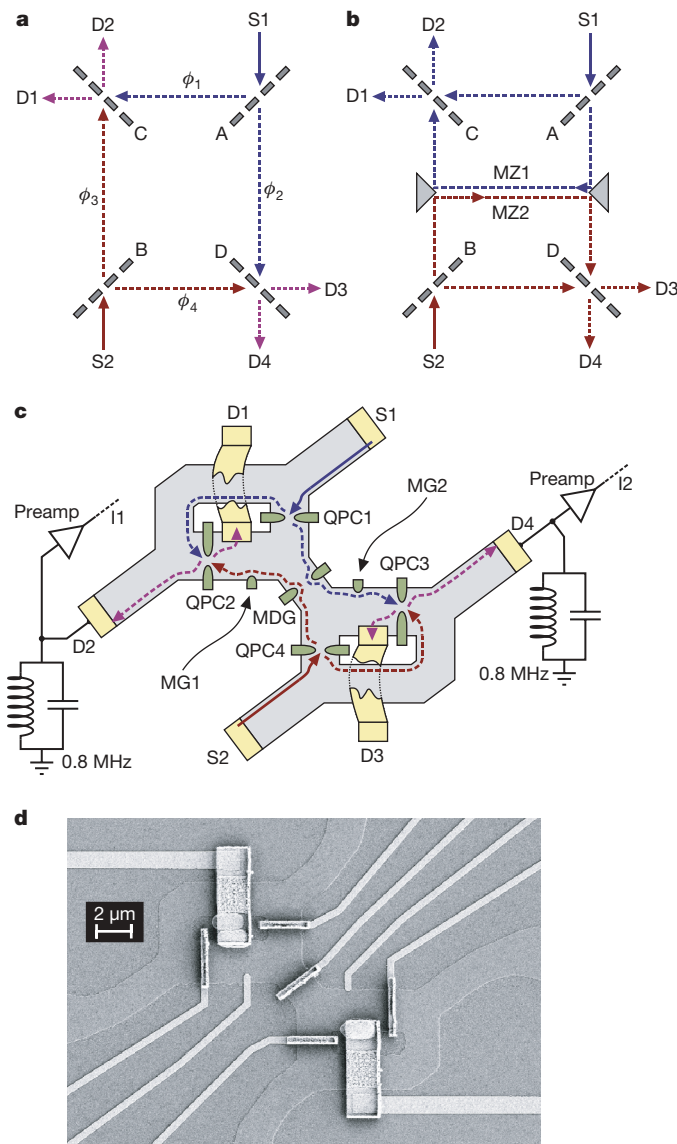


Figure 1 | The two-particle Aharonov-Bohm interferometer. **a**, Diagram of the interferometer. Sources S1 and S2 inject streams of particles, which are split by beam splitters A and B, later to recombine at beam splitters C and D. Each particle can arrive at any of four different drains, D1–D4. Each of the four trajectories accumulates phase ϕ_i . **b**, By breaking the interferometer in the centre, two separate Mach-Zehnder interferometers (MZIs) are formed. The MZIs are the building blocks of the two-particle interferometer. **c**, A detailed drawing of the interferometer. It was fabricated on a high mobility GaAs-AlGaAs heterostructure, with a two-dimensional electron gas buried some 70 nm below the surface (carrier density $2.2 \times 10^{11} \text{ cm}^{-2}$ and low temperature mobility $5 \times 10^6 \text{ cm}^2 \text{ V}^{-1} \text{ s}^{-1}$). Samples were cooled to $\sim 10 \text{ mK}$ electron temperature. Quantum point contacts (QPCs) served as beam splitters, and ohmic contacts as sources and drains. Tuning gates MG1 and MG2 changed the area and thus the magnetic flux threaded through the interferometer (at filling factor one of the integer quantum Hall effect). ‘Middle gate’ MDG separated the interferometer into two MZIs. Metallic air bridges connected drains D1 and D3 to the outside, where they were grounded. Currents at D2 and D4 were filtered first by an LC circuit (tuned to 0.8 MHz and 60 kHz bandwidth) and then amplified by a cold preamplifier (at 4.2 K). **d**, Scanning electron micrograph of the actual sample. Air bridges were used to contact the small ohmic contacts, the split gates of the QPCs, and the MDG.

with $\Phi_{\text{total}} = \phi_1 - \phi_3 + \phi_4 - \phi_2$, which is exactly the total accumulated phase going anti-clockwise along the four trajectories of the two particles.

Equation (3) describes the two-particle interference effect, with the absolute value squared of the prefactor of $\psi_{D_i D_j}$, the joint probability of having one electron at D_i and one at D_j . Concentrating on the correlation between D2 and D4, one can deduce from equation (3) the following: (1) two electrons never arrive at the same drain (Pauli exclusion principle); (2) the first part suggests that there is a 50% chance for two electrons to arrive at the same ‘side’ simultaneously, namely, at D1 and D2, or at D3 and D4, but never at D2 and D4; (3) the second part suggests that there is a 50% chance for two electrons to arrive at opposite ‘sides’, namely, one at D1 or D2 and the other at D3 or D4; however, the exact correlation depends on Φ_{total} . When $\Phi_{\text{total}} = \pi$, $\sin^2(\Phi_{\text{total}}/2) = 1$ and two electrons arrive at (D1, D3) or at (D2, D4), but when $\Phi_{\text{total}} = 0$, $\cos^2(\Phi_{\text{total}}/2) = 1$ and the complementary events take place. (4) Combining all events in the two parts of the total wavefunction, one finds for $\Phi_{\text{total}} = 0$ a perfect anti-correlation between the arrival of electrons in D2 and in D4; however, for $\Phi_{\text{total}} = \pi$ there is 50% chance of anti-correlation (first part) and 50% chance of positive correlation (second part)—hence, zero correlation. The time-averaged cross-correlated signal of the current fluctuations in the two drains is proportional to the probability of the correlated arrival of electrons in these drains. Varying the total phase should result in a negative oscillating cross-correlation signal between current fluctuations in D2 and in D4. The quantitative estimate of the amplitude of that cross-correlation signal is discussed later.

Figure 1b describes the realization of the experiment. The two-particle interferometer is shown split in the centre, resulting in an upper and lower segments; each is a simple optical Mach-Zehnder interferometer (MZI)¹⁸. An electronic version of the MZI has been recently fabricated and studied^{15,19,20}. A quantizing magnetic field ($\sim 6.4 \text{ T}$) brings the two-dimensional electron gas into the quantum Hall effect state at filling factor one. The current is carried by a single edge channel along the boundary of the sample¹⁶. Being a chiral one-dimensional object, the channel is highly immune to back scattering and dephasing. The layout of the two-particle interferometer is described in Fig. 1c, with the scanning electron micrograph of the actual device shown in Fig. 1d. The two MZIs can be separated from each other with a ‘middle gate’ (MDG). When it is closed, each MZI can be tested independently for its coherence and the Aharonov-Bohm periodicity. A quantum point contact (QPC), formed by metallic split gates, functions as a beam splitter while ohmic contacts serve as sources and drains. In this configuration, the phase that is accumulated along the four trajectories is the Aharonov-Bohm phase (φ_{AB}), namely, $\Phi_{\text{total}} = \varphi_{AB} = 2\pi BA/\Phi_0$, with B the magnetic field and A the area enclosed by the four paths ($\Phi_0 = 4.14 \times 10^{-15} \text{ T m}^2$ is the flux quantum)²¹. Look, for example, at the upper MZI of the separated two-particle interferometer (Fig. 1b). An edge channel, emanating from ohmic contact S1, is split by QPC1 into two paths that enclose a high magnetic flux and join again at QPC2. The phase dependent transmission coefficient from S1 to D2 is:

$$T_{\text{MZI}} = |t_{\text{QPC1}} t_{\text{QPC2}} + e^{i\varphi_{AB}} r_{\text{QPC1}} r_{\text{QPC2}}|^2 = T_0 + T_\varphi \cos(\varphi_{AB}) \quad (4)$$

where t and r are the transmission and reflection amplitudes of the QPCs. The visibility is defined as the ratio between the phase-dependent and the phase-independent terms, $v_{\text{MZI}} = T_\varphi/T_0$. The Aharonov-Bohm phase was controlled by the magnetic field and the ‘modulation gate’ (MG1 or MG2) voltage V_{MG} , which affected the area enclosed by the two paths.

Figure 2 displays the measured conductance of the two separated MZIs (defined as $i_D/V_S = T_{\text{MZI}}(e^2/h)$, where i_D is the AC current in the drain, V_S the applied a.c. voltage at the sources, with e^2/h the edge channel conductance). Pinching off MDG, the QPCs were tuned to transmission 0.5 and the AC signal was measured at D2 and D4 as a function of V_{MG} and magnetic field. As V_{MG} was scanned repeatedly

the magnetic field decayed unavoidably (as the superconducting magnet is not ideal) at a rate of $\sim 1.4 \text{ G h}^{-1}$. Hence, the interference pattern was 'tilted' in the two-coordinate plane of V_{MG} and time (magnetic field), with two basic Aharonov–Bohm periods for each MZI¹⁵. Apparently, the seemingly identical MZIs had different periodicities: 1 mV and 80 min in the upper MZI, and 1.37 mV and 87 min in the lower MZI (the asymmetry resulted from misaligning the QPCs and modulation gates). In the two MZIs, we found visibilities 75–90%, by far the highest measured in an electron interferometer. The high visibility was likely to result from the smaller size of the MZIs^{15,19,20}; hence, dephasing mechanisms such as flux fluctuations or temperature smearing were less effective. Moreover, the high quality two-dimensional electron gas assured a better formation of one-dimension-like edge channels and better overlap of particle wavefunctions.

We then discharged MDG, thus opening it fully and turning the two MZIs into a single two-particle interferometer. The conductances at D2 and D4 were now found to be independent of the Aharonov–Bohm flux, with a visibility smaller than the background ($< 0.1\%$). This is expected, as each electron did not enclose an Aharonov–Bohm flux any more.

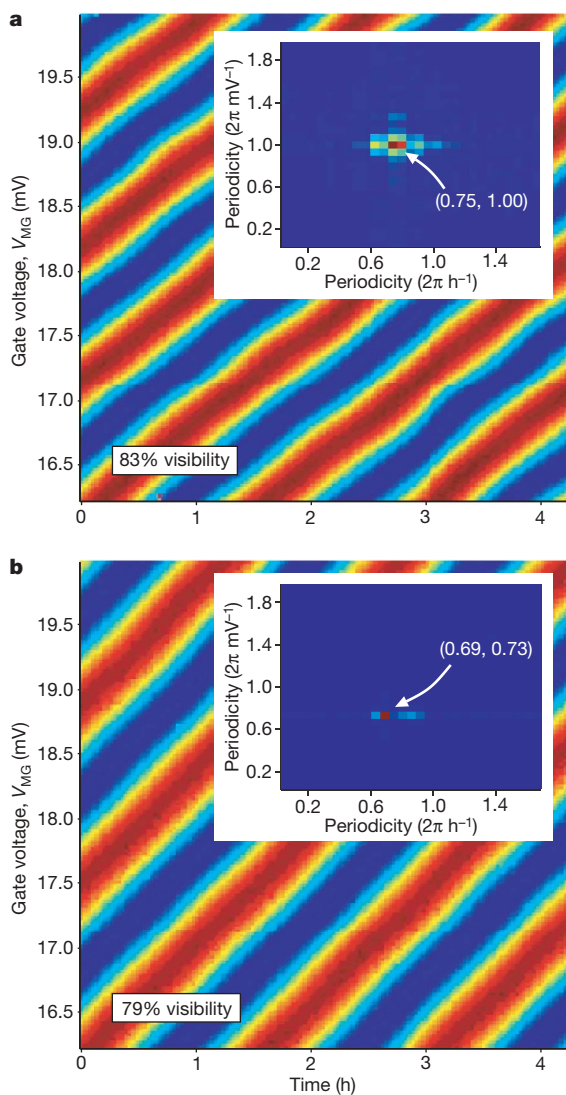


Figure 2 | Colour plot of the conductance of the two separate MZIs as function of the modulation gate voltage and the magnetic field that decayed in time. Strong Aharonov–Bohm oscillations dominate the conductance with visibilities of $\sim 80\%$ each. A two-dimensional FFT in the inset provides the periodicity in modulation gate voltage (V_{MG}) and in time.

We turn now to discuss the current fluctuations, namely, the shot noise in D2 and in D4. Feeding a d.c. current into S1, the low frequency spectral density of the shot noise in the partitioned current (by QPC1) at D2 and at D4 (with QPC2 closed and QPC3 and MDG open) was measured. Its expected value (neglecting here finite temperature corrections) is $S_{\text{D2}} = 2eI_{\text{S1}}T_{\text{QPC1}}(1 - T_{\text{QPC1}}) = 0.5eI_{\text{S1}}$ ($\text{A}^2 \text{ Hz}^{-1}$) for $T_{\text{QPC1}} = |t_{\text{QPC1}}|^2 = 0.5$ (ref. 15). The current fluctuations in the drain were filtered by an LC circuit, with 60 kHz bandwidth around a centre frequency $\sim 0.8 \text{ MHz}$, and then amplified by the cold amplifier, followed by a room-temperature amplifier and a spectrum analyser. In order to calibrate the cross-correlation measurement, we performed three noise measurements: (1) noise measured at D2; (2) noise measured at D4; and (3) noise measured by cross-correlating the current fluctuations at D2 and at D4 (by an analogue home-made correlating circuit). Measurements (1) and (2) both led accurately to the expected result above (they are anti-correlated and equal signals), which were used to calibrate measurements (3). An electron temperature of $\sim 10 \text{ mK}$ was deduced from these measurements²².

We were ready at this point to measure the two-particle cross-correlation. All four QPCs were tuned to $T_{\text{QPC}} = 0.5$ while the MDG was left open, hence, turning the two MZIs into a single two-particle interferometer. Equal DC voltages were applied to sources S1 and S2 with two separated power supplies $V_{\text{S1}} = V_{\text{S2}} = 7.8 \mu\text{V}$ ($I_{\text{S1}} = I_{\text{S2}} \equiv I = 0.3 \text{ nA}$). For that voltage, there is at most a single electron in each of the four trajectories of the interferometer (the wave packet's width, $15\text{--}30 \mu\text{m}$, estimated from the current and the estimated drift velocity ($\sim 3\text{--}6 \times 10^6 \text{ cm s}^{-1}$), is bigger than the interferometer's path length, being $\sim 8 \mu\text{m}$). This guaranteed a stronger overlap between the wavefunctions of the two electrons, and minimized Coulomb interaction among the electrons (thus eliminating nonlinear effects in the interferometer¹⁹). The measured fluctuations in D2 and D4 were averaged over some 30,000 electrons, amplified by two separate amplification channels (each fed by its own power supply), and finally cross-correlated. In order to verify

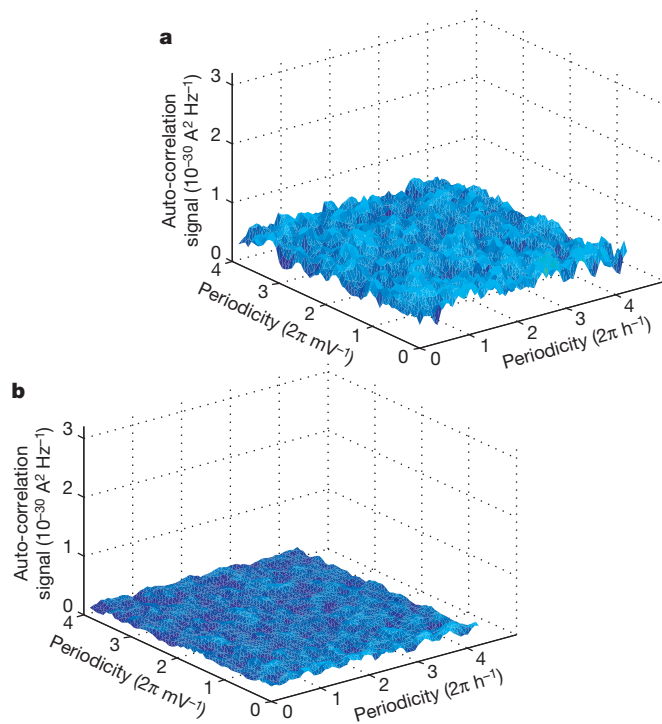


Figure 3 | Analysis and two-dimensional FFT of auto-correlation (shot noise) for an open 'middle gate'. Panels a and b show two-dimensional FFTs of shot noise measurements in D2 and D4, respectively. The noise is totally featureless, with no sign of Aharonov–Bohm oscillations above the background.

flux insensitivity in each drain separately, we first measured the shot noise in D2 and in D4 as function of the magnetic flux (varying V_{MG} and magnetic field). The noise, with a spectral density of $S = 0.5eI \approx 2.4 \times 10^{-29} \text{ A}^2 \text{ Hz}^{-1}$, was found to be featureless. For further assurance, a two-dimensional fast Fourier transform (FFT) of the measurements was calculated, with the results shown in Fig. 3a and b. Again, the transforms were without any feature above our measurement resolution of $\sim 2 \times 10^{-31} \text{ A}^2 \text{ Hz}^{-1}$, confirming the absence of flux periodicity in the noise (as was found also in the transmission).

We estimate now the expected magnitude of the cross-correlation signal from equation (3). When $\Phi_{\text{total}} = 0$, a maximum anti-correlation signal of the current fluctuations at the drains $S_{\text{D2D4}} = \langle \Delta I_{\text{D2}} \Delta I_{\text{D4}} \rangle$ is expected. It can be shown that the expected value of the cross-correlation spectral density, for a 100% visibility, is the same as that of the noise of a single QPC, that is, $S_{\text{QPC}} = 2eIT_{\text{QPC}}(1 - T_{\text{QPC}})$, or $0.5eI$ (for $T_{\text{QPC}} = 0.5$). As for $\Phi_{\text{total}} = \pi$ the cross-correlation signal is expected to vanish, we may conclude that the cross-correlation signal should oscillate with Φ_{total} , $S_{\text{D2D4}} = -0.25eI(1 - \sin \Phi_{\text{total}})$, with amplitude $1.2 \times 10^{-29} \text{ A}^2 \text{ Hz}^{-1}$ for $I = 0.3 \text{ nA}$.

Without currents in the sources, the cross-correlation signal was featureless (the background), with an average over the two-dimensional

FFT of $\sim 2 \times 10^{-31} \text{ A}^2 \text{ Hz}^{-1}$ (not shown). The cross-correlation measurement with $I = 0.3 \text{ nA}$ is shown in Fig. 4. The Aharonov–Bohm oscillations are already visible in the raw data (Fig. 4a bottom panel). In the two-dimensional FFT (Fig. 4b), one sees a sharp peak corresponding to a period of 0.58 mV in V_{MG} (with the same voltage applied to MG1 and MG2) and a period of 42.5 min in time (being proportional to the magnetic field decay). The square root of the integrated power under the FFT peak (the amplitude of the Aharonov–Bohm oscillations) is $3.0 \times 10^{-30} \text{ A}^2 \text{ Hz}^{-1}$. A roughly similar magnitude was observed also at a bulk filling factor of 2. Moreover, we could directly resolve the Aharonov–Bohm oscillations as a function of V_{MG} and time separately by coherent time averaging. As the magnetic field decayed in time, thus adding continuously an Aharonov–Bohm phase, this extra phase could be compensated for by shifting subsequent scans in V_{MG} according to the decay rate found in the two-dimensional FFT, leading to the negative oscillatory cross-correlation fringes shown in the top left panel of Fig. 4a. Similarly, the oscillations as a function of magnetic field have been extracted (top right panel, Fig. 4a). In Fig. 4c we provide the vector representation of the periodicities (inverse of periods) of each individual MZI (from Fig. 2) and that of the two-particle interferometer, the last being, quite accurately, the sum of the two. This is expected, as the rate of change of the Aharonov–Bohm flux

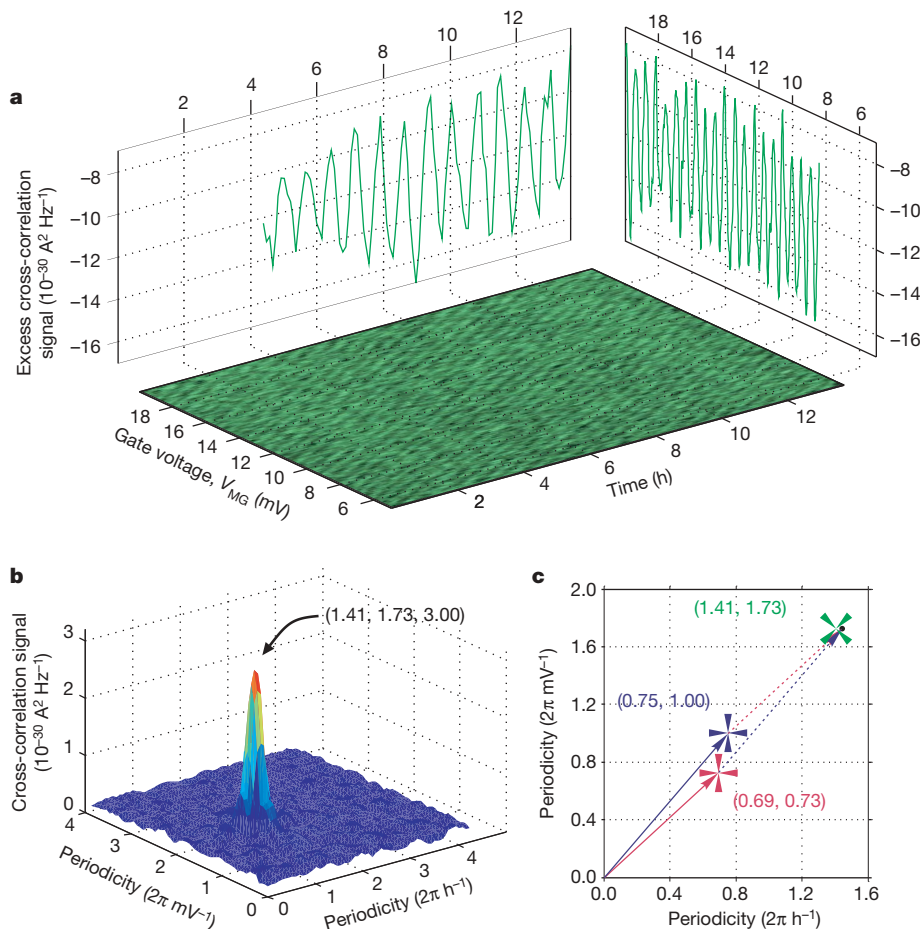


Figure 4 | Cross-correlation of the current fluctuations in D2 and D4.

a, Bottom, two-dimensional colour plot of the raw data as function of V_{MG} and time (magnetic field). The periodicity is already visible in the raw data. Top right panel, coherent averaging of some 50 traces as function of V_{MG} , by correcting for the added phase due to the decaying magnetic field (see text). Strong Aharonov–Bohm oscillations are seen in the negative excess cross-correlation (the part of the cross-correlation above the background, resulting from an injected current of 0.3 nA at each source). Note that the mean non-oscillating part of the excess cross-correlation is $-1.2 \times 10^{-29} \text{ A}^2 \text{ Hz}^{-1}$, as expected. Top left panel, similar averaging of the data but at a fixed V_{MG} . The somewhat different visibilities in both panels are

due to analysis that must be done in different regions of the two-dimensional plot. **b**, Two-dimensional FFT of the cross-correlation signal. A strong peak is visible, with an integrated power $3.0 \times 10^{-30} \text{ A}^2 \text{ Hz}^{-1}$. **c**, A vector representation of the different periodicities. The two vectors starting from the origin and ending at the blue and red crosses are the two-dimensional periodicities of the two MZIs. The green cross is the two-dimensional periodicity of the cross-correlation signal of the two-particle interferometer. The vectorial sum of the periodicities of the two MZIs (black dot) agrees excellently with the corresponding two-dimensional periodicity of the two-particle interferometer.

of the two-particle interferometer is the sum of the rates of the two MZIs.

Compared with the expected amplitude of the cross-correlation oscillations, $1.2 \times 10^{-29} \text{ A}^2 \text{ Hz}^{-1}$, we measured an amplitude of $3.0 \times 10^{-30} \text{ A}^2 \text{ Hz}^{-1}$. Our results are reasonably accurate, as the measurements have been repeated a few times and over long periods of integration times, lowering the uncertainty to below $10^{-31} \text{ A}^2 \text{ Hz}^{-1}$. At least two factors could lead to the lower cross-correlation signal. First, although we have no theory for it, it is likely that the lower visibility in each of the MZI's, v_{MZI1} and v_{MZI2} , will lower the cross-correlation signal by $v_{\text{MZI1}} \times v_{\text{MZI2}}$. Whereas the visibilities at zero applied d.c. voltage were $\sim 80\%$ (Fig. 2), the visibilities at the applied DC voltage $V_S = 7.8 \mu\text{V}$ were found to be $\sim 70\%$ (ref. 19). Second, our finite temperature ($\sim 10 \text{ mK}$) will lower the shot noise by $\sim 22\%$, affecting the cross-correlation signal similarly. These two effects alone will lower the expected cross-correlation signal to $\sim 4.6 \times 10^{-30} \text{ A}^2 \text{ Hz}^{-1}$, which is about 1.5 times higher than the measured one. This discrepancy is still not understood.

Our direct observation of interference between independent particles provides a reliable scheme to entangle separate, but indistinguishable, quantum particles. The present demonstration, done with electrons, reproduces the original Hanbury Brown and Twiss experiments^{13,14}, which were performed with classical waves. Such experiments are central to the study of the wavefunctions of multiple particles. Our scheme has the potential to test Bell inequalities^{2,3,23}; however, taking into account the finite temperature, it seems that the possibility of violating Bell inequalities in our measurements (with a visibility of merely 25%) requires further theoretical analysis.

Received 8 February; accepted 22 May 2007.

1. Feynman, R. P., Leighton, R. B. & Sands, M. *The Feynman Lectures on Physics* Vol. III, *Quantum Mechanics* (Addison-Wesley, New York, 1965).
2. Yurke, B. & Stoler, D. Bell's-inequality experiments using independent-particle sources. *Phys. Rev. A* **46**, 2229–2234 (1992).
3. Samuelsson, P., Sukhorukov, E. V. & Buttiker, M. Two-particle Aharonov-Bohm effect and entanglement in the electronic Hanbury Brown-Twiss setup. *Phys. Rev. Lett.* **92**, 026805 (2004).
4. Einstein, A., Podolsky, B. & Rosen, N. Can quantum-mechanical description of physical reality be considered complete? *Phys. Rev.* **47**, 777–780 (1935).
5. Mandel, L. Quantum effects in one-photon and two-photon interference. *Rev. Mod. Phys.* **71**, S274–S283 (1999).
6. Klitenbaek, R. *et al.* Experimental interference of independent photons. *Phys. Rev. Lett.* **96**, 240502 (2006).
7. Kumar, A. *et al.* Experimental test of the quantum shot noise reduction theory. *Phys. Rev. Lett.* **76**, 2778–2781 (1996).
8. Oliver, W. D., Kim, J., Liu, R. C. & Yamamoto, Y. Hanbury Brown and Twiss-type experiment with electrons. *Science* **284**, 299–301 (1999).
9. Henny, M. *et al.* The fermionic Hanbury Brown and Twiss experiment. *Science* **284**, 296–298 (1999).
10. Klessel, H., Renz, A. & Hasselbach, F. Observation of Hanbury Brown-Twiss anticorrelations for free electrons. *Nature* **418**, 392–394 (2002).
11. Reznikov, M., Heiblum, M., Shtrikman, H. & Ma'halu, D. Temporal correlation of electrons: Suppression of shot noise in a ballistic quantum point contact. *Phys. Rev. Lett.* **75**, 3340–3343 (1995).
12. Gavish, U., Levinson, Y. & Imry, Y. Shot-noise in transport and beam experiments. *Phys. Rev. Lett.* **87**, 216807 (2001).
13. Hanbury Brown, R. & Twiss, R. Q. A new type of interferometer for use in radio astronomy. *Phil. Mag.* **45**, 663–682 (1954).
14. Hanbury Brown, R. & Twiss, R. Q. Correlation between photons in two coherent beams of light. *Nature* **177**, 27–29 (1956).
15. Ji, Y. *et al.* An electronic Mach-Zehnder interferometer. *Nature* **422**, 415–418 (2003).
16. Halperin, B. I. Quantized Hall conductance, current-carrying edge states, and the existence of extended states in a two-dimensional disordered potential. *Phys. Rev. B* **25**, 2185–2190 (1982).
17. Lesovik, B. G. Excess quantum shot noise in 2D ballistic point contacts. *JETP Lett.* **49**, 592–594 (1989).
18. Born, M. & Wolf, E. *Principles of Optics* 7th edn 348–352 (Cambridge Univ. Press, Cambridge, UK, 1999).
19. Neder, I. *et al.* Unexpected behavior in a two-path electron interferometer. *Phys. Rev. Lett.* **96**, 016804 (2006).
20. Neder, I. *et al.* Entanglement, dephasing and phase recovery via cross-correlation measurements of electrons. *Phys. Rev. Lett.* **98**, 036803 (2007).
21. Aharonov, Y. & Bohm, D. Significance of electromagnetic potentials in quantum theory. *Phys. Rev.* **115**, 485–491 (1959).
22. Heiblum, M. Quantum shot noise in edge channels. *Phys. Status Solidi B* **243**, 3604–3616 (2006).
23. Bell, J. S. On the Einstein, Podolsky, Rosen paradox. *Physics* **1**, 195–200 (1964).

Acknowledgements We thank Y. Imry, U. Gavish, M. Buttiker, P. Samuelsson and D. Rohrlich for discussions. The work was partly supported by the Israeli Science Foundation (ISF), the Minerva foundation, the German Israeli Foundation (GIF), the German Israeli Project cooperation (DIP), and the Ministry of Science - Korea Program. Y.C. was supported by the Korea Research Institute of Standards and Science (KRISS), the Korea Foundation for International Cooperation of Science and Technology (KICOS), the Nanoscopia Center of Excellence at Hanyang University through a grant provided by the Korean Ministry of Science and Technology, and by the Priority Research Centers Program funded by the Korea Research Foundation.

Author Information Reprints and permissions information is available at www.nature.com/reprints. The authors declare no competing financial interests. Correspondence and requests for materials should be addressed to M.H. (heiblum@wisemail.weizmann.ac.il).